

Interferometer ^{12}CO observations of the box-shaped bulge spiral NGC 4013

S. García-Burillo¹, F. Combes², and R. Neri³

¹ Observatorio Astronomico Nacional (IGN), Apartado 1143, E-28800 Alcalá de Henares, Madrid, Spain (burillo@oan.es)

² Observatoire de Paris, DEMIRM, 61, Av. de l'Observatoire, Paris, France (bottaro@obspm.fr)

³ IRAM-Institut de Radio Astronomie Millimétrique, 300 Rue de la Piscine, F-38406 St. Mt. d'Hères, France (neri@iram.fr)

Received 25 September 1998 / Accepted 16 December 1998

Abstract. The nucleus of the box-shaped galaxy NGC 4013 has been observed with the IRAM interferometer in the J=1–0 and J=2–1 lines of ^{12}CO . Our maps show the existence of a fast-rotating (130 km s^{-1}) molecular gas disk of radius $r\sim 2''$ (110 pc). Several arguments support the existence of a bar potential in NGC 4013. The *figure-of-eight* pattern of the major axis p-v plot, the ring-like distribution of gas, and the existence of gas emission at non-circular velocities are best accounted by a bar.

We have also detected gas at high z distances from the plane ($z\sim 200\text{--}300\text{ pc}=4''\text{--}5''$). The latter component is related to a system of 4 $\text{H}\alpha$ filaments of diffuse ionized gas that come out from the nucleus. The galactic fountain model seems the best to account for the $\text{H}\alpha$ and CO filaments. Although the peanut distortion can be spontaneously formed by a stellar bar in the disk, gas at high z might have been ejected after a nuclear starburst. The $\text{H}\alpha$ filaments start in the plane of the disk at $r\sim 200\text{ pc}(4'')$, and reach several Kpc height at $r\sim 600\text{ pc}(10'')$, coinciding with the maximum peanut distortion where the strength of the restoring forces of the plane have a minimum. We have critically examined other alternatives judged less probable: the existence of a CO warp (connected to the HI warping disk), the accretion of gas along stable inclined orbits and, finally, a vertical gas response near the resonances of the peanut (the latter is tested by numerical simulations).

Although a link between the bar and the box-shaped bulge in NGC 4013 is suggested we find noticeable differences between the results of previous numerical simulations and the present observations. The discrepancy concerns the parameters of the bar generating the peanut. We see in NGC 4013 the existence of a *strong* ILR region. The inclusion of a dissipative component, which remains to be thoroughly studied, may change the evolution of the stellar peanut: although in simulations the peanut appears initially near a *marginal* ILR, the inflow of gas driven by the bar, can make two ILRs appear.

Key words: galaxies: individual: NGC 4013 – galaxies: ISM – galaxies: kinematics and dynamics – galaxies: spiral

1. Introduction

N-body numerical simulations have established a link between the existence of boxy-shaped galaxy bulges and the presence of a bar instability in the disk (Combes and Sanders, 1981; Combes et al. 1990, hereafter called **C90**; Raha et al. 1991; Pfenniger and Friedli, 1991; Friedli and Martinet, 1993; Friedli and Benz, 1993). The bar can thicken, driven by vertical resonances, giving the bulge a boxy-shaped or peanut appearance, provided that the galaxy is seen at a high inclination ($i>70^\circ$), and depending on the orientation of the major axis of the bar with respect to the line of nodes (measured by the azimuth Φ): an edge-on bar ($\Phi=90^\circ$) adopts a boxy shape and the peanut feature appears for a large range of intermediate azimuths. The thickening is supported by star orbits that leave the galaxy plane and it occurs only in a *privileged* region along the bar where there is coincidence between the horizontal resonance ILR ($\Omega_b = \Omega - \kappa/2$) and its vertical counterpart ($\Omega_b = \Omega - \nu_z/2$). Other mechanisms, not related to the presence of a bar potential in the disk, can explain the formation of peanut bulges. Several authors support the merger/accretion interpretation (Binney and Petrou 1985, Shaw 1993, Shaw et al. 1993). The occurrence of dissipationless collapse of an isolated system (Lima-Neto and Combes 1995), possibly in the presence of a bound companion (May et al. (1985)) have also accounted for the existence of boxy shapes in galaxy bulges.

In view of the large variety of scenarios it is necessary to envisage a detailed comparison between the different models and the observations for specific objects. There are very few examples where the connection between bars and box-peanut bulges have been investigated from an observational point of view. Bettoni and Galletta 1994 found photometric evidence of a bar in the peanut spiral NGC 4442; Kuijken and Merrifield 1995 studied a sample of edge-on spirals using $\text{H}\alpha$ and optical lines as tracers of gas kinematics. However extinction effects can be severe in highly inclined disks where the column densities of gas and the associated dust can reach very high values. The use of *macroscopically* optically thin tracers such as CO can help us to get a more clear picture of the gas kinematics, especially in the central regions of these spirals. In particular, in this work we investigate the link between bars and box-peanut bulges using

CO as a fair tracer of the molecular gas kinematics in the nuclear disk of a candidate galaxy: NGC 4013.

The Sbc edge-on spiral NGC 4013 has been identified as an extreme box-peanut bulge object, as seen in the optical pictures of van der Kruit and Searle (1982) and Jarvis (1986). Rand (1996) (hereafter referred to as **R96**) have taken deep $H\alpha$ images of NGC 4013 searching for extraplanar diffuse ionized gas (DIG), discovering an impressive set of filaments coming out the plane in the nuclear region. He suggests this is the signature of a nuclear outflow, after a starburst episode related with the distorted morphology of the nucleus. NGC 4013 was mapped in the J=2–1 and 1–0 lines of ^{12}CO with the IRAM 30m telescope (HPBW $13''$ and $21''$, respectively) by Gómez de Castro and García-Burillo, 1997 (hereafter referred as **GCGB97**). The CO disk extends to $r=100''$ and it consists of a ring-like source (of radius $r=30\text{--}40''$) and an unresolved fast-rotating nuclear disk. The high-velocity CO component has no HI counterpart (see Bottema et al. 1987, Bottema 1995 and 1996) and it is best explained by **GCGB97** invoking the presence of a non-axisymmetric potential. Still the spatial resolution of the observations was insufficient to undertake a detailed analysis of gas kinematics in the nucleus of the galaxy. Furthermore the single-dish data suggested also the existence of *out-of-the-plane* gas that might be connected either with the vertical structure of the box-peanut bulge stable orbits, or the occurrence of an outflow and local ejections of material, as the DIG measurements of **R96** seem to indicate. High-resolution ($\sim 3''$) interferometer CO data of NGC 4013 are presented in this work, intending to study the distribution and kinematics of molecular gas in the nucleus of this galaxy and hopefully clarify the nature of the link between bars and box/peanut bulges.

The study of dynamics of the gas in a peanut potential will deserve detailed numerical simulations involving both the stars and the gas, to be fully presented in a forthcoming publication (paper II). In this paper we limited ourselves to analyse whether there is a spontaneous and stable vertical response of the gas to a peanut potential, using a first run of numerical simulations.

2. Observations

The $^{12}\text{CO}(1\text{--}0)$ observations were made with the IRAM interferometer of Plateau de Bure (see description in Guilloteau et al. 1992), between December 1995 and March 1996. During less than one third of the observing period we observed simultaneously the 2–1 line of ^{12}CO . We used the compact (CD) 4-antenna configurations, consisting of 18 baselines ranging from 24 to 180 m. The declination of the source ($\delta \sim 44^\circ$) allowed good UV coverage and made possible to synthesize an ellipsoidal beam of $\text{FWHM}=3.4'' \times 3.3''$ in the 1–0 line, adopting natural weighting and no taper on the visibilities ($\text{FWHM}=1.2'' \times 1''$ in the 2–1 line). The $^{12}\text{CO}(1\text{--}0)$ antenna half-power primary beam was $43''$ ($22''$ in the $^{12}\text{CO}(2\text{--}1)$). The primary beam field was centered at $\alpha(J2000)=11^{\text{h}}58^{\text{m}}31.7^{\text{s}}$, $\delta(J2000)=43^\circ 56' 48.1''$. Assuming a distance of 11.6 Mpc (Bottema 1995), the $43''$ primary beam corresponds to 2.4 kpc ($1''=56$ pc).

A total bandwidth of 430 MHz (1120 and 560 km s^{-1} for the 1–0 and 2–1 lines respectively), centered at $v=839$ km s^{-1} (LSR) and largely covering the range of velocities observed in NGC 4013 (± 250 km s^{-1} , according to **GCGB97**), was observed with a resolution of 2.5 and 1.25 MHz (6.5 km s^{-1} and 3.3 km s^{-1} at 115 and 230 GHz, respectively). The central 140 MHz of this band was also observed at 115 GHz with a resolution of 0.63 MHz (1.6 km s^{-1}).

Data calibration was made in the standard way using the CLIC software package (Lucas 1992). The correlator was calibrated every 20 min with a noise diode, and the RF passband once at the beginning of each observing run on 3C273. The relative phase of the antennas was checked every 20 min on the nearby quasars 1308+256 and 1156+295. The rms atmospheric phase fluctuations were typically between 10° and 25° at 115GHz.

The data were then cleaned to yield channel maps. The rms noise in a 2.5 MHz-wide channel is 2.3 mJy ($\Delta T_B=0.018$ K) per $3.35''^2$ beam at 115GHz (the $1\text{-}\sigma$ noise is of 20 mJy per beam in the 2–1 line or equivalently 0.35 K).

3. The CO maps

In the following, we will denote by x and z the kinematical major and minor axis of NGC 4013 (x increasing to the NE and z to the NW). All coordinates will be referred to the dynamical center (x_C, z_C) which has been determined as follows: we first fit the position angle of the galaxy (PA) together with the z_C position of the disk, applying a standard least-squares method to the integrated intensity map of fig2a. The inferred value for the orientation of the galaxy plane is $PA = 66^\circ \pm 5^\circ$, in agreement with the value derived from optical imaging. Finally both x_C and the systemic velocity v_{sys} are derived imposing the maximum symmetry on the the inner $10''$ region of major axis p–v plot taken at $z=z_C$. We calculate $(x_C, z_C)=(0,0)=\alpha(J2000.0) = 11^{\text{h}}58^{\text{m}}31^{\text{s}}.36$, $\delta(J2000.0) = 43^\circ 56' 50'' .9$. This position coincides within $1''$ with the radio-continuum sources detected at 6 cm and 21 cm (note that Bottema (1995) reports a wrong position for the radio-continuum source) as well as with the optical center determined by Palumbo et al. 1988. Similarly, the velocities (v) will be relative to $v_{sys}=840 \pm 10$ km s^{-1} (LSR).

Fig. 1 shows the $^{12}\text{CO}(1\text{--}0)$ velocity-channel maps observed with the interferometer (oriented along x and z axes). Emission appears from $v=143$ to -170 km s^{-1} , concentrated in a rotating edge-on disk whose vertical structure is marginally resolved with our $3.4''$ beam. However we notice ‘out of the plane’ gas excursions mostly in the bottom-left quadrant (within the range $\Delta x=(-5'', 25'')$ and $\Delta z=(-3'', -8'')$), visible at certain velocities (within the range $\Delta v=(-20$ $\text{km s}^{-1}, -105$ km s^{-1}).

At the derived dynamical center offset (0,0), CO emission displays a large spread of velocities: ± 130 km s^{-1} . As shown in Fig. 2a, which represents the $^{12}\text{CO}(1\text{--}0)$ velocity-integrated temperature map, the observed high-velocity gas at the center is linked with the presence of a conspicuous CO nuclear disk in the inner 100 pc ($2''$). The nuclear disk shows an east-west asymme-

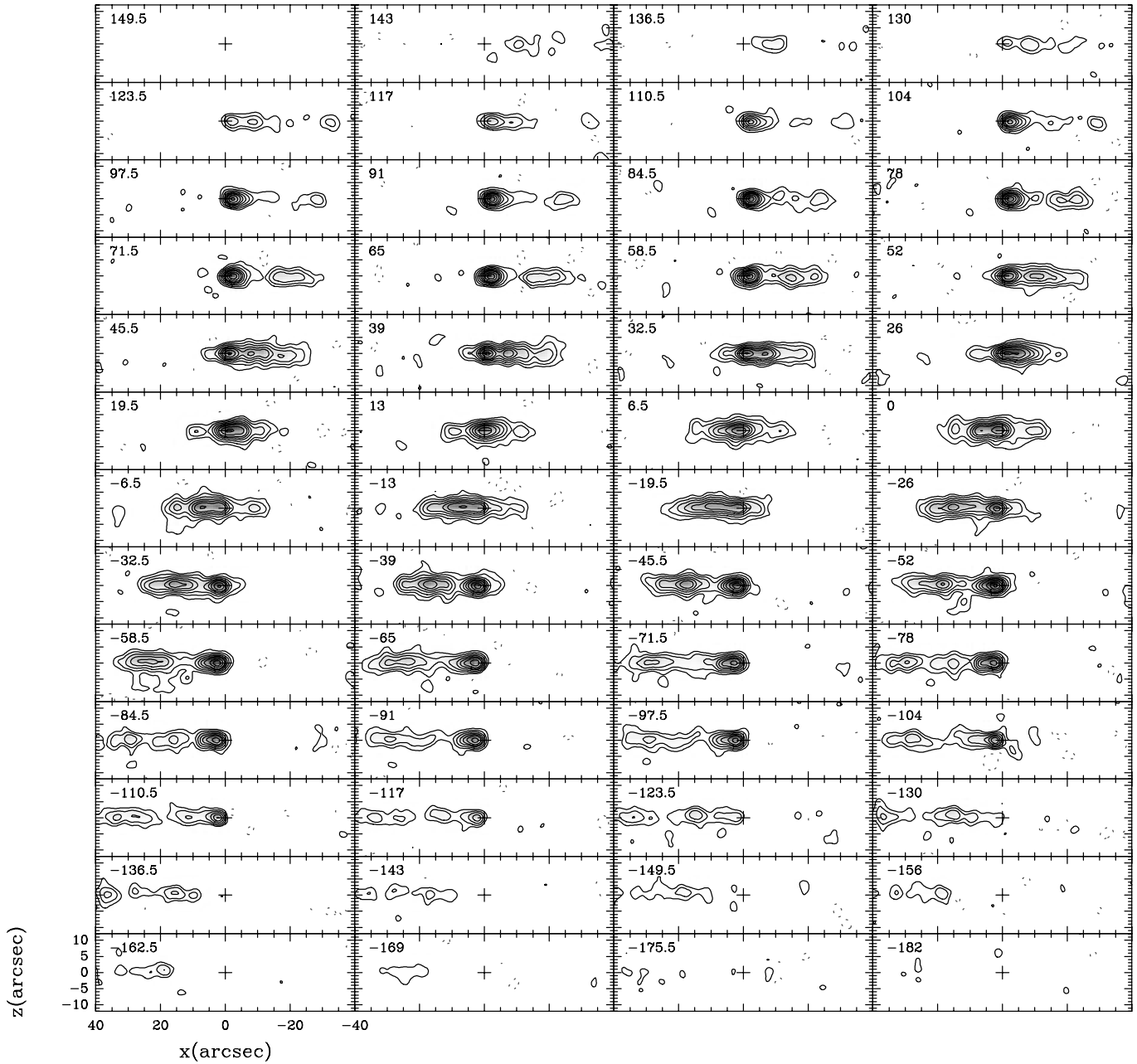


Fig. 1. $^{12}\text{CO}(1-0)$ velocity-channel maps observed with the Plateau de IRAM interferometer with a resolution (HPBW) of $3.4'' \times 3.1''$. Coordinates are with respect of the dynamical center (indicated by the cross). Velocity-channels range from $v=150 \text{ km s}^{-1}$ to $v=-182 \text{ km s}^{-1}$ by steps of 6.5 km s^{-1} . Contour levels are $-12, 12, 24, 40, 60, 80, 100$ to $200 \text{ mJy beam}^{-1}$ by steps of 30 mJy beam^{-1} .

try: the maximum of emission is located at $x \sim 2''$, i.e., eastwards with respect to the dynamical center. The remarkable asymmetry of the inner 100 pc of NGC 4013 is more clearly shown by the higher resolution 2–1 data: Fig. 2b shows the velocity-integrated map in the 2–1 line which allows to resolve the nuclear disk radially. The latter displays an asymmetrical ring-like structure of radius $r \sim 1.7''$ (95 pc).

The overall distribution of molecular gas in the disk shows a similar E-W asymmetry with respect to (0,0): CO is stronger and it is more extended in the eastern side, up to $x=35''$, than in the western side of the disk, up to $x=-25''$ (the single-dish

data of **GCGB97** already showed this asymmetry holds for radii $40'' < r < 100''$). The same asymmetry is echoed by other star formation tracers ($\text{H}\alpha$ and non-thermal radiocontinuum). A similar asymmetry in the CO distribution is present in the inner nucleus of our Galaxy (Bally et al. 1987, 1988) and other spirals (see the case of NGC 891: García-Burillo and Guélin, 1995).

3.1. The mass of molecular gas

If we take a CO to H_2 conversion factor of $X = \text{N}(\text{H}_2)/I_{\text{CO}} = 2.3 \times 10^{20} \text{ cm}^{-2} \text{ K}^{-1} \text{ km}^{-1} \text{ s}$ (Strong et al. 1988), the

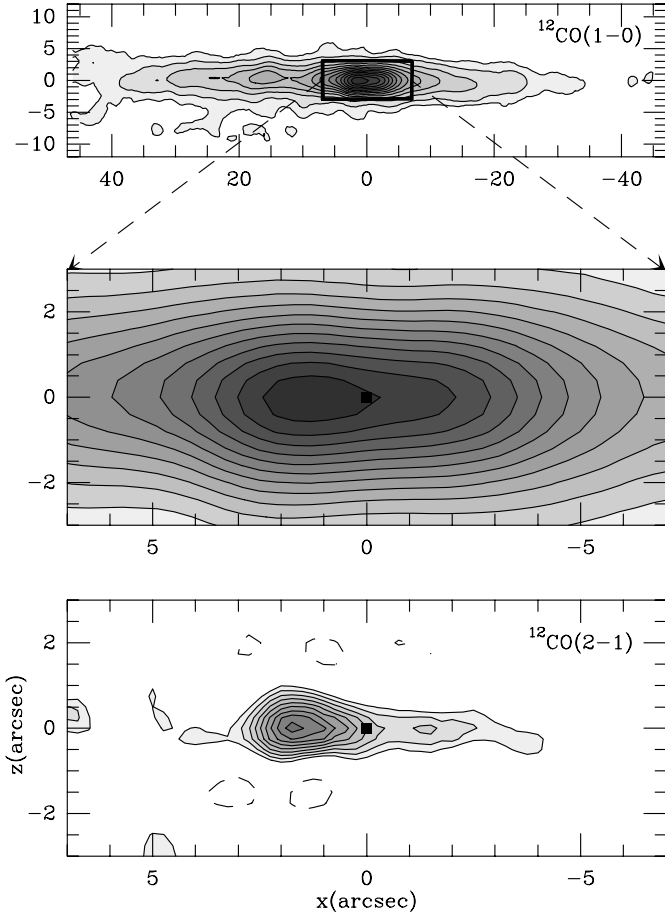


Fig. 2. **a** (top): $^{12}\text{CO}(1-0)$ integrated intensity contours observed with the IRAM interferometer towards the center of NGC 4013. x and z are offsets (in arcsec) with respect to the dynamical center **C**. Contours are 1 and 2 to $24 \text{ Jy km s}^{-1} \text{ beam}^{-1}$, by steps of $2 \text{ Jy km s}^{-1} \text{ beam}^{-1}$. A zoomed view of **a** is displayed below. **b** (bottom): same as **a** but for the 2–1 line of ^{12}CO . Contours are 4 to 15 by $1 \text{ Jy km s}^{-1} \text{ beam}^{-1}$.

H_2 mass derived from the $^{12}\text{CO}(1-0)$ interferometer map is $M(\text{H}_2) = 3 \times 10^8 M_\odot$. For this we assumed the distance to be $D = 11.6 \text{ Mpc}$ and integrated the CO flux within a rectangular area of dimensions $70'' \times 18''$, centered on the position $(0,0)$. Including the mass of Helium, the total molecular gas mass in the Bure field is $M_{gas} = M(\text{H}_2 + \text{He}) = 4 \times 10^8 M_\odot$. The nuclear disk mass content is derived to be close to $M_{gas} \sim 0.6 \times 10^8 M_\odot$ (this is an upper limit as we integrated I_{CO} within $r = 2''$ for all velocities, including the contribution of gas seen in projection close to $(0,0)$ but located far from the nucleus in the plane of the galaxy).

Taking into account that the shortest spacing measured by the interferometer is $\sim 20 \text{ m}$, we expect to filter scales $\langle L \rangle \sim 20\text{--}25''$ at 115 GHz (equivalently, $\langle L \rangle \sim 10\text{--}15''$ at 230 GHz). We have derived the fraction of the single-dish $^{12}\text{CO}(1-0)$ and $(2-1)$ fluxes included in the Bure maps. The zero-spacing flux filtered out by the interferometer is kept very low in the 1–0 line: we detect nearly $\sim 100\%$ of the 30m-flux within the interferometer primary beam. On the contrary, the

filtering is severe at 230 GHz : we estimate that $\sim 1/2$ of the 30m flux is missing in the 2–1 primary beam.

4. The vertical distribution of molecular gas

Assuming the vertical distribution to be gaussian-like we have derived the thickness of the CO disk (Δz) deconvolving the measured FWHM on the $^{12}\text{CO}(1-0)$ velocity-integrated intensity map of Fig. 2a by our $3.4'' \times 3.3''$ synthesized beam. The inferred Δz shows no systematic radial trend along the major axis and it varies between $1.5''$ and $2.5''$, i.e. translated into spatial scales $\Delta z = 80\text{--}130 \text{ pc}$. These values are comparable with the thickness of the thin molecular gas disk in the Galaxy: $60\text{--}100 \text{ pc}$ (Bronfman et al. 1988).

The existence of CO emission at high z is clearly visible in the bottom left quadrant of Fig. 2a (see also Fig. 3a). Note that the lowest contour corresponds to $5 \times \sigma_A$, where a value of $\sigma_A = 0.2 \text{ Jy beam}^{-1} \text{ km s}^{-1}$, has been obtained through the expression $\sigma_A = \int_{\Delta v} \sigma dv$, taking $\sigma = 0.002 \text{ Jy beam}^{-1}$ and $\Delta v = 100 \text{ km s}^{-1}$. The mass of molecular gas at high z is $M(\text{H}_2) \sim 1.5 \times 10^7 M_\odot$, ($\sim 5\text{--}10\%$ of the total emission). The latter is a conservative lower limit as the CO-to- H_2 conversion factor might be significantly higher. The existence of vertical extensions of molecular gas in the nucleus was already suggested by **GCGB97** using coarse resolution single-dish data.

The connection between the DIG filaments discovered by **R96** and the above reported CO extraplanar emission is best illustrated at certain velocities. Figs. 3b–c–d represent an overlay of a K-band image of NGC 4013, showing the peanut bulge distortion of the nucleus in the region $(\Delta x, \Delta z) = (\pm 15'', \pm 10'')$ with the CO-velocity channel maps at $v = -26, -52$ and -104 km s^{-1} (Figs. 3b, 3c and 3d, respectively). A sketch of the DIG filaments of **R96** is included for comparison. **R96** interpreted the impressive set of 4 DIG filaments above and below the nucleus of NGC 4013 as the signature of a massive nuclear starburst. Supernova explosions might inject a huge amount of energy to the gas finally lifted to high z . At close sight, filament A is associated with CO emission breaking out of the plane ($v = -26 \text{ km s}^{-1}$), although extraplanar gas appears to be more spread above the plane than the DIG feature (see $v = -52 \text{ km s}^{-1}$ and Fig. 3a). Filament B is also associated with extraplanar CO ($v = -104 \text{ km s}^{-1}$).

We have estimated the gravitational potential energy of the extraplanar molecular gas associated with filament A (the most impressive), using the inferred positions of CO emission above the mid-plane. Taking the two isothermal stellar components model of Jacobi and Kegel (1994), fitted on the luminosity distribution out of the plane in NGC 4013, the resultant gravitational energy per unit mass Φ is

$$\Phi = \sigma_i^2 \ln \cosh(z/h)$$

$$\sigma_i^2 = (\rho_1 \sigma_1^2 + \rho_2 \sigma_2^2) / (\rho_1 + \rho_2)$$

where ρ_i and σ_i stand for the stellar mid-plane densities and velocity dispersions of the $i=1,2$ components and h is the fitted scale height ($h = 1.72 \text{ kpc}$ and $\sigma_i = 58.3 \text{ km s}^{-1}$ for NGC 4013, according to Jacobi and Kegel (1994)). The average height of

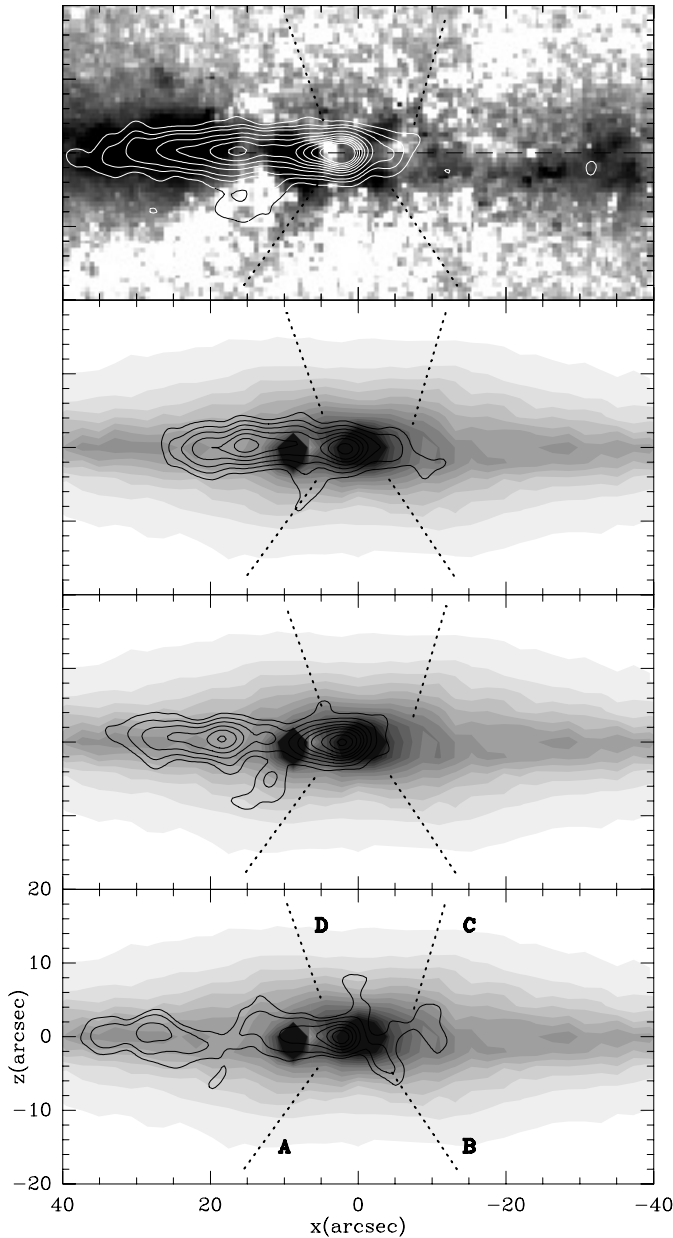


Fig. 3. a (top panel) We overlay the $H\alpha$ extraplanar emission image of **R96** showing the existence of 4 DIG filaments (grey scale) with the map of CO emission integrated within the velocity range $\Delta v = (0 \text{ km s}^{-1}, -80 \text{ km s}^{-1})$ (contours). We show an overlay of the $^{12}\text{CO}(1-0)$ velocity-channel maps at $v = -26 \text{ km s}^{-1}$ **b** (top), $v = -52 \text{ km s}^{-1}$ **c** (middle) and $v = -104 \text{ km s}^{-1}$ **d** (bottom) (contours) with a K band image of the nucleus of NGC4013 taken from Shaw 1993 (gray scale contours). A sketch of the 4 extraplanar DIG $H\alpha$ filaments is depicted in **a–d** (dashed lines).

the CO extraplanar emission observed within the interval $v = -13, -78 \text{ km s}^{-1}$ is $z \sim 270 \text{ pc}$, which gives a total potential energy of $50 \times 10^{51} \text{ ergs}$ for $M_{gas} = 4 \times 10^6 M_{\odot}$. We emphasize that the above equation allows to calculate the total potential energy of the material at height z , and therefore should be taken as a lower limit to the total input energy that must be given to the molecular gas in the plane to reach the observed values: first we have

not considered the kinetic energy of these gaseous structures at present and we made no assumptions on the efficiency of the mechanism which is responsible for injecting the energy to the gas in the plane. Whatever the nature of this energy source is, at least 50 type II supernovae are required (assuming that a type II supernova releases $\sim 10^{51} \text{ ergs}$ to the ISM). This lower limit might transform into an order of magnitude higher number of required SN, once the radiative and dissipative energy losses of the process are taken into account, henceforth suggesting that the nucleus of NGC 4013 might be experiencing a starburst episode. On the other hand, the restoring force of the galaxy plane is diminished near the position of the maximum distortion of the potential and this limit can be slightly lowered.

The FIR indices in NGC 4013 do not indicate a massive starburst at the global scale of the disk: neither the normalised infrared fluxes, $\log(\text{FIR}/a_{gal}^2) = -13.8$ (where a_{gal} is the galaxy major axis in arcminutes) and $\log(\text{FIR}/L_B) = 0.3$, nor the IRAS colors ($S_{25}/S_{12} = 1.5$; $S_{100}/S_{25} = 30$) are indicative of typical starbursts (see Huang et al., 1996 for discussion of a large galaxy sample). However there is evidence that supports a starburst event in the nucleus: first, a huge fraction ($\sim 30\%$) of the total radio-continuum flux at 21 cm is emitted by the nuclear disk; this fraction is the highest among the sample of galaxies published by Hummel et al. 1991. Most noticeably, there is an association between the H-shape of the DIG filaments and extraplanar CO emission with the box-peanut appearance of the bulge. A similar set of filaments has been discovered by Rand in a galaxy also classified as a box-peanut: NGC 3079. Connection between the nuclear starburst, the distorted stellar potential and the CO kinematics is discussed below (Sects. 5 and 6).

HI observations (Bottema 1995) showed the existence of a highly warped disk in NGC 4013. CO emission at high z present in our observations could come from regions of the outer warped disk seen in projection near the nucleus. However a comparison of velocity channel maps of atomic and molecular gas leads us to reject this explanation: whereas CO emission at high z appears at negative velocities in the bottom left quadrant (Figs. 2–3), the HI warp shows up in the top left quadrant (NE in Fig. 2 of Bottema 1995) within the same velocity range.

5. Kinematics of molecular gas

Fig. 4a shows the $^{12}\text{CO}(1-0)$ position-velocity diagram taken along the major axis. The high-inclination of the galaxy allows us to get the whole range of radial velocities in the plane. Molecular gas emission is spread in a rhomboid-like region where we distinguish three velocity components:

- I The most outstanding component displays a large spread of velocities ($v = \pm 130 \text{ km s}^{-1}$) towards the dynamical center (referred to as the straight ridge C) and it has no HI counterpart. The high-velocity gas corresponds to the central CO nuclear disk identified in Figs. 2a-b and it extends from $x = -3''$ to $x = 3''$. It is fully resolved in the 2–1 line where it extends from $x = -2''$ to $2''$; note that dv/dr reaches a maximum value of $\sim 1000 \text{ km s}^{-1} \text{ kpc}^{-1}$ in the inner 100 pc ($2''$).

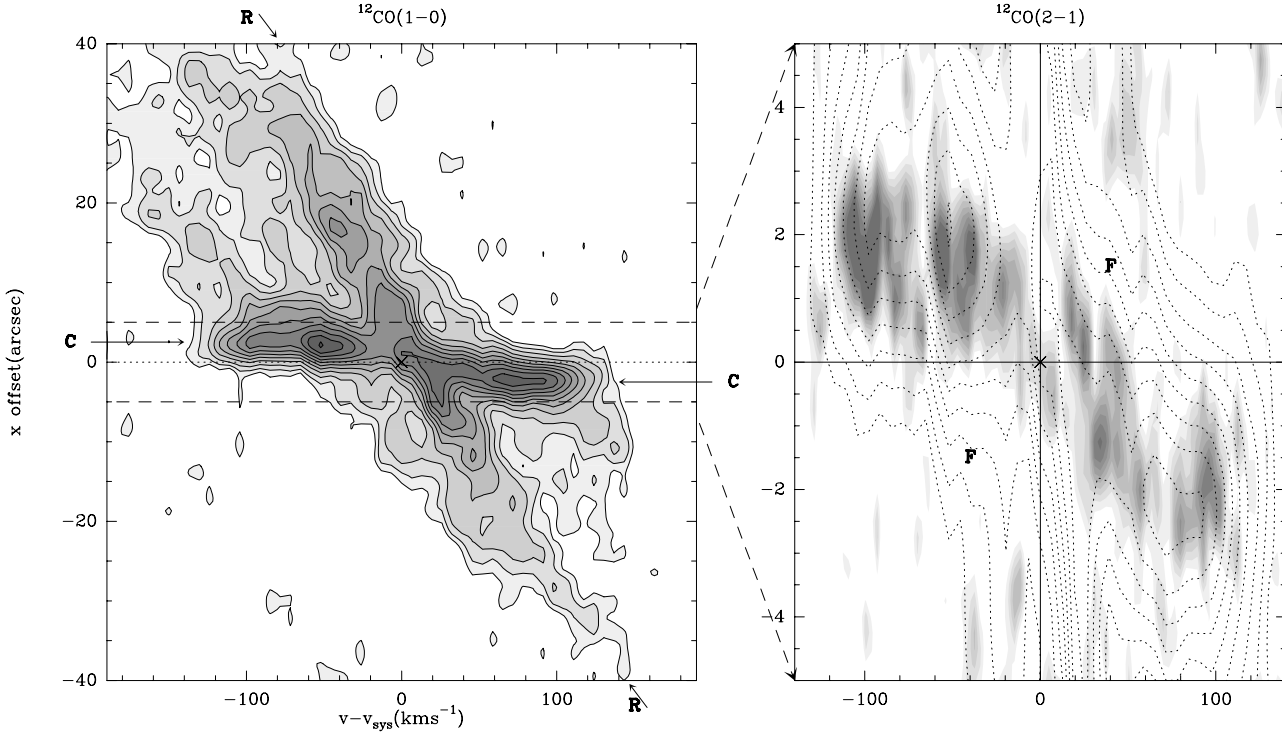


Fig. 4. a (left): The $^{12}\text{CO}(1-0)$ position-velocity diagram along the kinematical major axis, oriented along $\text{PA}=66^\circ$. Gray contours correspond to 0.010, 0.020, 0.035 to $0.200 \text{ Jy beam}^{-1}$ by steps of $0.02 \text{ Jy beam}^{-1}$. A zoomed view on the inner $r=5''$ region, where there is a CO nuclear disk showing high-velocity gas, is displayed on the right. **b** (right): same as **a** but now for the 2–1 line of ^{12}CO with a $\sim 1''$ resolution in gray scale contours, linearly scaled from 0.035 to $0.200 \text{ Jy beam}^{-1}$ by steps of $0.025 \text{ Jy beam}^{-1}$. Dashed contours stand for the same $^{12}\text{CO}(1-0)$ position-velocity diagram shown in **a**. Notation of kinematical components (**C**, **R** and **F**) are explained in text.

- II Part of the emission is concentrated in a straight ridge (**R**) which slowly drifts in velocity when we move along the major axis: it extends from $(x=30'', v=-80 \text{ km s}^{-1})$ to $(x=-30'', v=100 \text{ km s}^{-1})$. HI emission is detected in this region of the p-v plot according to Bottema et al. 1987, Bottema 1995 and 1996. CO emission fills unevenly the p-v space between **C** and **R**.
- III We detect gas at non-circular velocities (or velocities *forbidden* by circular rotation) in the inner $\pm 5''$. This region (**F**) extends symmetrically on both sides of the nucleus: at $x \sim -3.5''$, we measure CO emission up to $v \sim -60 \text{ km s}^{-1}$, whereas circular rotation would impose $v > 0$ for $x < 0$. The same applies for the offset $x \sim 3.5''$ where $v \sim 60 \text{ km s}^{-1}$.

5.1. The major axis p-v profile

We have derived the CO-based rotation curve (v_{rot}^{CO}) from the terminal velocities method, applied to the p-v major axis diagram. We have used the 2–1 data in the inner $x = \pm 2''$, the 1–0 data from $2'' < x < 25''$, and finally added the 30m data of **GCGB97** for the outer disk ($25'' < x < 100''$). In the derivation, we have taken into account the effect of channel smearing ($\Delta v = 6.5 \text{ km s}^{-1}$) and assumed a typical cloud-cloud velocity dispersion of $\sim 10 \text{ km s}^{-1}$. Finally we have assumed that v is translatable into v_{rot}^{CO} , as circular-motions should be the main contributor to v (Sofue 1996; García-Burillo 1997).

Note that the HI-based rotation curve (v_{rot}^{HI}) cannot account for the CO high-velocity gas component **C**. The scarcity of atomic hydrogen in the nucleus, together with the low resolution of HI observations can explain the differences between v_{rot}^{HI} and v_{rot}^{CO} . We therefore conclude that the real rotation curve is certainly much steeper in the inner $20''$ than inferred using HI data: $v_{rot}^{CO} = 110 \text{ km s}^{-1}$ at $r = 110 \text{ pc}$, this implies a dynamical mass of $M_{dyn} = r \times v_{rot}^2 / G = 2.8 \times 10^8 M_\odot$, assuming a spheroidal component in the nuclear region (a factor 0.6 lower in the case of a flat disk distribution). Therefore, we estimate M_{gas}/M_{dyn} to be of 22% inside the nuclear disk. The latter ratio goes down monotonically to reach 10% at $r = 500 \text{ pc}$. Although the dynamics is still dominated by the stars, the contribution of molecular gas to the total mass content of the nuclear disk is significantly high and the effects of gas self-gravitation might not be negligible.

As stated above, the **F** component indicates the existence of emission at non-circular velocities. The high-resolution of the present observations precludes any explanation of **F** in terms of beam dilution: at $x = \pm 3.5''$ we are off by more than one synthesized beam from the center.

5.2. A bar in NGC 4013?

The presence of the **F** component is more readily explained by invoking a deviation from axisymmetry in the inner ($r \sim 200 \text{ pc}$) mass distribution of NGC 4013. More precisely, we have ob-

servational evidence that the gas flow in this galaxy might be driven by a barred potential:

- The major axis p-v diagram shown in Fig. 4a displays the *figure-of-eight* shape typical of gas flowing along a bar (Binney et al. 1991; García-Burillo and Guélin 1995; Kuijken and Merrifield 1995). Components **C** and **R**, producing a double-peaked line-of-sight velocity plot, would correspond to molecular gas populating two different families of orbits: x_2 inner orbits for **C**, and higher energy x_1 orbits for **R**. The **F** component is best explained as the projection of the outer x_1 orbits close to the cusped orbit. x_2 orbits develop between two inner Linblad resonances ILRs (the outer (oILR) and the inner (iILR)). x_1 orbits exist between the oILR and the corotation of the bar (COR). This particular morphology of the p-v plot cannot be reproduced if we impose axisymmetry in the potential (Kuijken and Merrifield 1995).
- Moreover we expect to see the imprint of a bar in the radial distribution of molecular gas as a reflect of secular evolution. Gravitational torques induce a radial redistribution of gas which accumulates in rings between the ILRs, the 4:1 or UHR resonance and the outer Linblad resonance (OLR). As a result, the corotation region is progressively emptied of gas. The radial distribution of gas in NGC 4013 shows a compact central source of radius $r \sim 2''$ (**C**), a region relatively emptied of gas between **C** and **R** ($r \sim 10\text{--}30''$) and a secondary maximum towards $r \sim 50''$ (according to the single-dish data of **GCGB97**). This distribution, showing the existence of several rings, is well accounted by the bar hypothesis.
- Fig. 6 shows the $^{12}\text{CO}(2-1)$ isovelocity contours in the nuclear disk region. The z-distribution of molecular gas is spatially resolved at $1''$ resolution: we detect the presence of a slight velocity gradient along the minor axis of the galaxy and a westwards tilt of $\sim 60^\circ$ in the isovelocities of the nuclear disk, suggesting that we are seeing in projection a non-axisymmetric gas distribution.

Although the arguments enumerated above cannot be taken as a proof of the existence of a barred potential, it all points out to this scenario as the simplest explanation. To explore on more firm grounds the consequences of this hypothesis, in the following section we try to locate the main resonances of the bar in the disk.

5.3. Inferring limits on the bar pattern speed

The standard first-order approach consists in deriving the principal frequencies of the disk from the fitted rotation curve (v_{rot}^{CO}): Ω , $\Omega - \kappa/2$, $\Omega + \kappa/2$ and $\Omega + \kappa/4$ (see Fig. 5). Assuming the epicyclic approximation, we can figure out the value of the bar pattern speed (Ω_p) and consequently the position of the main resonances, based on observational and theoretical arguments. This procedure is not intended to provide an accurate fit of Ω_p , but to test if the basic results of numerical simulations are supported by the present observations.

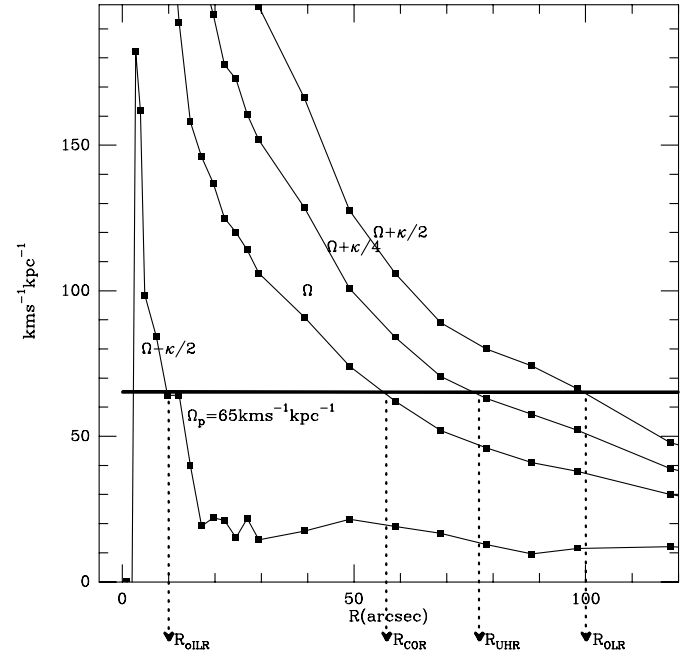


Fig. 5. The radial variation of main frequencies of NGC 4013 (Ω , $\Omega - \kappa/2$, $\Omega + \kappa/2$ and $\Omega + \kappa/4$) is plotted, assuming the epicyclic approximation and based on the CO rotation curve. The loci of the principal resonances are determined for a value of $\Omega_p = 65 \text{ km s}^{-1} \text{ kpc}^{-1}$.

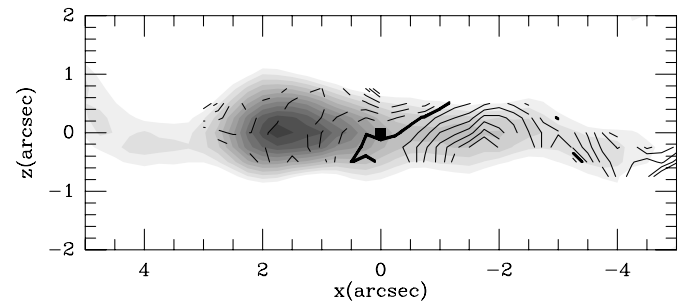


Fig. 6. The $^{12}\text{CO}(2-1)$ isovelocity contours (solid and dashed lines) in the nuclear disk of NGC 4013, linearly spaced from -100 km s^{-1} to 100 km s^{-1} by steps of 20 km s^{-1} , overlaid on the corresponding integrated intensity map (Fig. 2b).

As shown in Fig. 5, the $\Omega - \kappa/2$ curve presents a strong maximum ($\sim 180 \text{ km s}^{-1} \text{ kpc}^{-1}$) at $r \sim 3.5''$ and it goes monotonically down to 1/10 of its peak value ($\sim 20 \text{ km s}^{-1} \text{ kpc}^{-1}$) at $r \sim 20''$; farther out, it stays quite flat until the edge of the optical disk. Self-consistent numerical simulations of bars, including only the stellar component (**C90**), predict that the formation of the peanut occurs when the bar breaks up the plane near a *marginal* ILR (i.e., the bar pattern speed remains always close to the maximum of $\Omega - \kappa/2$). If this is to apply in NGC 4013, we would require the bar to have an unlikely high pattern-speed ($\Omega_p > 180 \text{ km s}^{-1} \text{ kpc}^{-1}$) which also implies a *marginal* ILR at $r \sim 4''$. The latter is not compatible with the observations: the maximum distortion of the peanut bulge in NGC 4013 is at $r \sim 12''$. Moreover, as we ignore a priori the orientation of the

bar major axis along the line of sight, $r \sim 12''$ should be taken as a lower limit for the ILR.

Most of the available numerical simulations have treated the appearance of the peanut distortion and its evolution including only the stars. Although the influence of a dissipative component on the fate of the peanut remains to be studied thoroughly, a plausible evolutionary sequence can be advanced here. The peanut instability first sets in at a *marginal* ILR of the bar, but this should be taken as a starting point. The subsequent inwards flux of gas towards the original ILR, driven by the bar's gravitational torque, can change the $\Omega - \kappa/2$ curve in the inner region. The curve can become progressively steeper and finally two inner Lindblad resonances (outer (oILR) and inner (iILR)) are bound to appear. The stellar bar itself is expected to slightly slow down in the process. The peanut distortion is the relic of an old *marginal* ILR; however a *strong* ILR region will develop in the course of time. Any reasonable value of Ω_p in NGC 4013 implies we have two ILRs at present: an inspection of Fig. 5 leads to that conclusion unavoidably. Therefore, the existence of a peanut instability and a *strong* ILR region in the nucleus may not be in contradiction, but should be taken as a result of secular evolution. Numerical simulations to be developed in paper II will allow us to test this scenario.

Fitting the bar pattern speed is beyond the scope of the present paper, however a lower limit on Ω_p can be tentatively set. The radial distribution of molecular gas (with a relative depression or hole between $r=10''$ and $r=30''$) suggest that corotation cannot be at a radius larger than $r \sim 50''$, implying that $\Omega_p > 60\text{--}70 \text{ km s}^{-1} \text{ kpc}^{-1}$. The latter implies the following loci of principal resonances: $r_{iILR} > 2''$, $r_{oILR} < 12''$, $r_{COR} < 50''$, $r_{UHR} < 70''$ and $r_{OLR} < 100''$. Corotation of the bar is kept well inside the optical disk. This is expected for bars in spirals of early or intermediate Hubble types such as NGC 4013, classified as Sbc (see Combes and Elmegreen 1993). Secondly, if $\Omega_p > 60\text{--}70 \text{ km s}^{-1} \text{ kpc}^{-1}$, the oILR appears inside the old marginal ILR (at $12''$), as proposed lines above. Finally the major axis distribution of CO showing a maximum at $r \sim 50''$ is well accounted for if a ring forms near the UHR resonance ($r_{UHR} < 70''$).

6. A link between the gas filaments and the bar?

In a barred and peanut-shaped potential, the gas in principle tends to follow the periodic orbits, and is dragged through vertical resonances out of the plane, like the stars. However, the gas is dissipative, on a short time-scale; cloud-cloud collisions occur with a characteristic collision time of 10^7 yr. While the peanut and perpendicular elevation time scale is a long process, of time-scale almost 10^9 yr (C90). Therefore, the gas component loses its disordered kinetic energy, and in particular in the z-direction, rather quickly. The gas settles down in a very thin disk, irrespective of the peanut-shape potential.

In order to study if there can be a stable and spontaneous vertical response of gas in a peanut potential, we have performed self-consistent numerical simulations involving gas and stars. In this first run, the gas mass fraction is kept very low on purpose

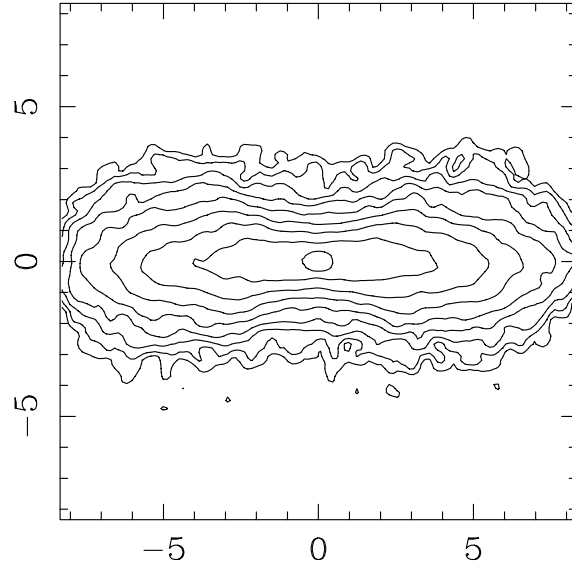


Fig. 7. Contours of stellar projected density of the bar seen edge-on, after 4 Gyr of simulation. The scale is in kpc.

($\sim 2\%$). The gas clouds are considered as sticky particles and we neglected the effects of self-gravitation. No effect of star formation on the gas dynamics is considered either. The code used is FFT-based particle-mesh, with the gas treated as sticky particles (Combes & Gerin 1985). The useful grid is $128 \times 128 \times 64$, and the suppression of the Fourier images is done through the algorithm of James (1977). The run included 150k stellar particles and 40k gas particles. A bar forms spontaneously in the stellar component, since the bulge to disk mass ratio is $1/3$, and there is no other spheroidal component that could stabilize the disk. After 2×10^9 yr, the bar has developed a characteristic peanut shape (see contours of Fig. 7). The main result is that, at any time, the gas disk remains very thin (~ 200 pc at half-power), and is never perturbed by the peanut/shaped potential or only in a very transient manner (see Fig. 8).

The vertical thickening of the bar and the subsequent formation of the peanut can be caused by instabilities associated with resonances between the bar motion and the vertical oscillations of the stars (C90; see also Binney (1981)); this effect has also been attributed to the buckling or fire-house instability by Raha et al. 1991. The bar instability first acts to increase the eccentricity of stellar orbits and align their principal axes; this causes the buckling instability, precisely about the vertical resonance region, which increases vertical velocity dispersion and thickness. Once the bar is thickened, the nature of the stellar orbits in the peanut can be described with orbits trapped around the 2:2:1 periodic orbit family: these correspond to the vertical Lindblad resonance, where in the frame of the bar, the particles just perform two z-oscillations in one turn ($\Omega - \nu_z/2 = \Omega_b$, the bar pattern speed). This happens to occur in the region of the in-plane inner Lindblad resonance (where $\Omega - \kappa/2 = \Omega_b$), and therefore the resonant orbits have the 3-D shape of a banana (projected into an ellipse in the plane (C90, Pfenniger & Friedli 1991). A detailed orbital study has emphasized the bifurcations

of the main periodic orbits x_1 onto the banana and anti-banana orbit families (Pfenniger & Friedli 1991). These periodic orbits, in a strong bar, very often possess loops, and the gas is not likely to follow them because of dissipation. This may explain the small propensity of the gas to be elevated vertically, at least for directly rotating orbits. For retrograde orbits, on the contrary, the orbit family x_4 bifurcates due to vertical instability into the anomalous orbits (corresponding this time to a 1/1 resonance, or one vertical oscillation for one turn, Pfenniger & Friedli 1991). This family does not possess loops, and the gas can be maintained more easily on these (Friedli & Benz 1993). These retrograde orbits could be populated in particular during an accretion event, where gas clouds arrive with a given angular momentum, un-correlated with that of the galaxy. The case of NGC 128 is a remarkable example. It is a peanut-shaped galaxy seen edge-on, where an inclined gaseous disk is observed to counter-rotate with respect to the stars (Emsellem & Arsenault 1997). Although this galaxy has apparently no sign of perturbed morphology, it has a companion nearby (NGC 127) which could have provided the retrograde gas.

These stable retrograde orbits are characteristic of a tumbling triaxial potential. Already van Albada et al. (1982) had remarked that in the rotating frame of a triaxial object, the Coriolis forces on retrograde particles produce a torque, which is opposite to and compensates the torque of the restoring forces towards the plane. The latter would have made the retrograde orbits to precess, and since they differentially precess with radius, the clouds' collisions and dissipation would have forced the gas to settle in the main plane. The Coriolis forces, therefore, stabilise the gas into the inclined retrograde orbits. These orbits are not particularly related to the peanut shape, but both phenomena indicate the presence of bars.

In NGC 4013, the presence of a prodigious warp (Bottema et al. 1987) suggests that a large amount of gas has recently been accreted with un-related angular momentum. Part of it could have gone towards the center. If spontaneously, directly-rotating gas will not stay at large height above the plane due to the peanut shape of the potential, it is possible that accreted gas with a different angular momentum, not aligned with the principal axis, could be trapped in banana orbits, or more likely in retrograde anomalous orbits. More simulations are needed, taking into account the accretion origin of the gas, and also its larger mass fraction and self-gravity (see paper II).

An alternative mechanism to explain the presence of gas at high altitude above the plane, is the galactic fountain effect, due to massive star formation. This could explain the morphology of the $H\alpha$ filaments, that appear much higher above the plane than the neutral gas, traced by the CO emission in the center. The fact that the filaments seem to coincide with the peanut region might not be a coincidence: the gas is easier to expel when the restoring force of the plane is less, i.e. in the thicker stellar plane.

Extraplanar neutral+ionized gas and dust have been found in another edge-on spiral: NGC 891. The existence of a thick molecular disk, containing $M(H_2) \sim 10^8 M_\odot$ up to $z \sim 1$ kpc, was first established by García-Burillo et al. (1992) using single dish

CO observations. **R96** also reports the detection of an extended DIG halo with some prominent $H\alpha$ filaments in this galaxy. Recently Howk and Savage (1997) have discovered the dusty counterpart of the thick CO disk: the HST and WIYN optical BVR images of NGC 891 show hundreds of dust filaments lying far from the mid-plane. The derived neutral gas mass content of these absorbing structures closely agrees with the CO-based estimates. Although some of the extraplanar dust features are interpreted as supernova-driven galactic chimneys, other are less clearly linked with highly energetic phenomena in the disk. In either cases, the existence of an extended neutral+ionized gas with a set of dust filaments is related to the high star formation efficiency in the disk (García-Burillo et al. 1992; **R96**; Howk and Savage 1997).

7. Summary and conclusions

We have observed with the IRAM interferometer the emission of the 1–0 and 2–1 lines of ^{12}CO in the nucleus of NGC 4013, an edge-on Sbc spiral possessing a box-shaped bulge, with spatial resolutions of $\sim 3.3''$ and $\sim 1.2''$, respectively.

Our maps show the presence of a distinct fast-rotating ($v_{rot} \sim 130 \text{ km s}^{-1}$) nuclear disk of radius $r \sim 2''$ (100 pc) and gas mass $M_{gas} \sim 0.6 \times 10^8 M_\odot$. The high-velocity component (absent in the HI map) is accompanied by gas emission at non-circular velocities within $\pm 3''$ from the dynamical center, indicating that the gas flow is driven by a non-axisymmetrical potential. An analysis of the gas kinematics, derived from the $^{12}\text{CO}(1-0)$ major axis position-velocity plot and the $^{12}\text{CO}(2-1)$ isovelocities map, supports a bar model for NGC 4013. The observed ring-like distribution of molecular gas (at $r \sim 2''$ (100 pc) and $r \sim 50''$ (2.7 kpc); the outer ring inferred from the 30m map) is interpreted as the imprint of a bar.

Although a link between the bar and the box-shaped bulge in NGC 4013 is suggested, there are apparent discrepancies between the results of numerical simulations and the model proposed here. Disagreement concerns the basic parameters of the bar generating the peanut. In self-consistent simulations of the star component the peanut forms near the locus of a *marginal* ILR of the bar. Instead, the derived $\Omega - \kappa/2$ curve in NGC 4013 leaves little doubt of the existence of a *strong* ILR response, irrespective of the chosen pattern speed of the bar (Ω_p). The nuclear disk would be located in the vicinity of the iILR, with no gaseous ring counterpart in the oILR. The present observations suggest that the inclusion of a dissipative component in simulations might probably change the evolution of the stellar peanut: although the latter appears near a marginal ILR, the inflow of gas driven by the bar, makes two ILRs appear and accelerates the secular evolution of the gaseous disk in the inner ~ 1 kpc region of the galaxy. Numerical simulations, involving both the stars and the gas in a peanut potential, will analyse the response of the gas in the disk of the galaxy fully testing the bar hypothesis (see paper II).

We analysed the vertical distribution of molecular gas, showing that, although the bulk of CO emission comes from a thin disk (with deconvolved thickness FWHM $\sim 80-130$ pc),

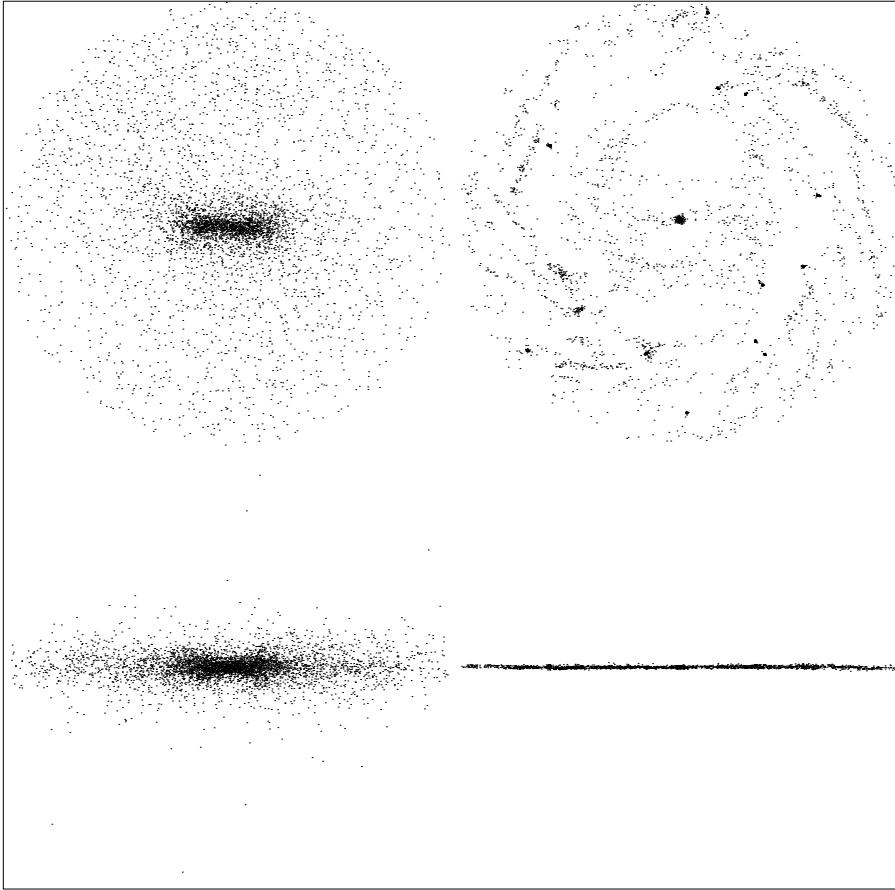


Fig. 8. Particle plots at the same epoch (4 Gyr) of the stars (*left*) and gas (*right*). Up is the face-on view, and bottom the edge-on view. In each frame, the maximum radius is 25 kpc.

there is a non-negligible amount of molecular gas ($M(\text{H}_2) = 1.5 \times 10^7 M_\odot$) at large z distances from the plane ($z \sim 200\text{--}300$ pc). The close relationship between the DIG filaments seen in $\text{H}\alpha$ coming out of the plane and the presence of molecular gas emission, suggests that both share a common origin: gas ejected by a massive nuclear starburst.

A preliminary run of simulations has restricted to study the vertical response of the gas to a peanut potential, that spontaneously forms in a disk of stars. Gas clouds are treated as test particles and we neglect here the effects of star formation and self-gravity in the gas dynamics. Due to its dissipative nature, the gas forms a thin disk very quickly. Contrary to the stars, the gas cannot be maintained at high altitude above the galaxy plane along stable orbits. Cloud-cloud collisions make impossible the population of banana and antibanana self-intersecting orbits. Moreover, it remains to be studied if gas clouds can populate the vertical bifurcation of the retrograde x_4 family in a peanut, after an accretion episode (see paper II). However this mechanism is unlikely to hold for NGC 4013, where the bulk of the gas in the disk is directly rotating.

Among the different explanations for the gas at high z -inclined resonant orbits connected to the peanut, gas accretion in the course of an interaction and, finally, the galactic fountain model—the latter seems the best to account for the $\text{H}\alpha$ and CO filaments. Although the peanut distortion formed in the stars comes from a bar in the disk (the presence of the latter being

suggested by the observed CO kinematics), gas is being ejected in the nucleus after a bar driven starburst. The filaments come from the inner 200 pc ($4''$) and reach a height of several Kpc, coinciding with the maximum peanut distortion where the strength of the restoring forces of the plane is diminished.

Acknowledgements. This work has been partially supported by the Spanish CICYT under grant number PB96-0104. The authors heartily thank Richard Rand for giving us the $\text{H}\alpha$ image of NGC 4013 used in this paper. We also would like to thank Martin Shaw for making available his K-band image. We finally thank James Binney, the referee, for his encouraging comments and criticisms.

References

- Bally J., Stark A.A., Wilson R.W., Henkel C., 1987, ApJS 65, 13
- Bally J., Stark A.A., Wilson R.W., Henkel C., 1988, ApJ 324, 223
- Bettoni D., Galletta G., 1994, A&A 281, 1
- Binney J., 1981, MNRAS 196, 455
- Binney J., Petrou M., 1985, MNRAS 214, 449
- Binney J., Gerhard O.E., Stark A.A., Bally J., Uchida K.I., 1991, MNRAS 252, 210
- Bottema R., Shostak G.S., van der Kruit P.C., 1987, Nat 328, 401
- Bottema R., 1995, A&A 295, 605
- Bottema R., 1996, A&A 306, 345
- Bronfman L., Cohen R.S., Alvarez H., May J., Thaddeus P., 1988, ApJ 324, 248
- Combes F., Sanders R.H., 1981, A&A 96, 164
- Combes F., Gerin M., 1985, A&A 150, 327

- Combes F., Debbash F., Friedli D., Pfenniger D., 1990, *A&A* 233, 82, (C90)
- Combes F., Elmegreen B.G., 1993, *A&A* 271, 391
- Emsellem E., Arsenault R., 1997, *A&A* 318, L39
- Friedli D., Benz W., 1993, *A&A* 268, 65
- Friedli D., Martinet L., 1993, *A&A* 277, 27
- García-Burillo S., Guélin M., Cernicharo J., Dahlem M., 1992, *A&A* 266, 21
- García-Burillo S., Guélin M., 1995, *A&A* 299, 657
- García-Burillo S., 1997, In: Sofue Y. (ed.) *IAU Symposium 184, The Central Regions of the Galaxy and Galaxies*. Kyoto-Japan. PASP, San Francisco, p. 116
- Gómez de Castro A.I., García-Burillo S., 1997, *A&A* 322, 381 (GCGB97)
- Guilloteau S., Delannoy J., Downes D., et al., 1992, *A&A* 262, 624
- Howk J.C., Savage B.D., 1997, *AJ* 114, 6
- Huang J.H., Gu Q.S., Su H.J., et al., 1996, *A&A* 313, 13
- Hummel E., Beck R., Dettmar R.-J., 1991, *A&AS* 87, 309
- Jacobi S., Kegel W.H., 1994, *A&A* 282, 401
- James R.A., 1977, *J.Comput.Phys* 25, 71
- Jarvis B.J., 1986, *AJ* 91, 65
- Kuijken K., Merrifield M.R., 1995, *ApJ* 443, L13
- van der Kruit P.C., Searle L., 1982, *A&A* 110, 61
- Lima-Neto G., Combes F., 1995, *A&A* 294, 657
- Lucas R., 1992, CLIC, IRAM document
- May A., van Albada T.S., Norman C.A., 1985, *MNRAS* 214, 131
- Palumbo G.G.C., et al., 1988, *Accurate Positions of Zwicky Galaxies*. October 1988, special version, SIMBAD
- Pfenniger D., Friedli D., 1991, *A&A* 252, 75
- Raha N., Sellwood, J.A., James R.A., Kahn F.D., 1991, *Nat* 352, 411
- Rand R.J., 1996, *ApJ* 462, 712, (R96)
- Shaw M., 1993, *MNRAS* 261, 718
- Shaw M., Wilkinson A., Carter D., 1993, *A&A* 193, 268, 511
- Sofue Y., 1996, *ApJ* 458, 120
- Strong A.W., Bloemen J.B.G.M., Dame T., et al., 1988, *A&A* 207, 1
- van Albada T.S., Kotanyi C.G., Schwarzschild M., 1982, *MNRAS* 198, 303